Shortcomings of InSAR for studying megathrust earthquakes: The case of the M_w9.0 Tohoku-Oki earthquake

Guangcai Feng[1] and Sigurjón Jónsson[1]

Received 7 March 2012; revised 19 April 2012; accepted 19 April 2012; published 22 May 2012.

[1] Interferometric Synthetic Aperture Radar (InSAR) observations are sometimes the only geodetic data of large subduction-zone earthquakes. However, these data usually suffer from spatially long-wavelength orbital and atmospheric errors that can be difficult to distinguish from the coseismic deformation and may therefore result in biased fault-slip inversions. To study how well InSAR constrains fault-slip of large subduction zone earthquakes, we use data of the 11 March 2011 Tohoku-Oki earthquake (M_w 9.0) and test InSAR-derived fault-slip models against models constrained by GPS data from the extensive nationwide network in Japan. The coseismic deformation field was mapped using InSAR data acquired from multiple ascending and descending passes of the ALOS and Envisat satellites. We then estimated several fault-slip distribution models that were constrained using the InSAR data alone, onland and seafloor GPS/acoustic data, or combinations of the different data sets. Based on comparisons of the slip models, we find that there is no real gain by including InSAR observations for determining the fault slip distribution of this earthquake. That said, however, some of the main fault-slip patterns can be retrieved using the InSAR data alone when estimating long wavelength orbital/atmospheric ramps as a part of the modeling. Our final preferred fault-slip solution of the Tohoku-Oki earthquake is based only on the GPS data and has maximum reverse- and strike-slip of 36.0 m and 6.0 m, respectively, located northeast of the epicenter at a depth of 6 km, and has a total geodetic moment is 3.6×10^{22} Nm (M_w 9.01), similar to seismological estimates. **Citation:** Feng, G., and S. Jónsson (2012), Shortcomings of InSAR for studying megathrust earthquakes: The case of the M_w9.0 Tohoku-Oki earthquake, *Geophys. Res. Lett.*, *39*, L10305, doi:10.1029/2012GL051628.

1. Introduction

[2] Fault slip models of earthquakes in subduction zones can be difficult to constrain well from geodetic data. The main problem is that onland observations usually exist from only one side of the fault (the hanging wall), acquired at a significant distance from the trench, resulting in limited model resolution. In addition, many subduction zone earthquakes are deep and produce limited surface deformation. On the other hand, we usually have information about the location and geometry of the fault from distribution of earthquakes taking place on the subduction interface between the two converging plates. This information allows us to fix the fault geometry and reduce the fault modeling to a linear problem of estimating only variations in fault slip.

[3] Another problem is limited data, as most subduction zones are not covered with continuously operating geodetic networks. This problem has been highlighted with many recent large subduction earthquakes [*Lorito et al.*, 2011]. Satellite radar interferometry (InSAR) provides a potential solution to this problem with its global coverage and high spatial sampling [*Tong et al.*, 2010]. InSAR imaging does, however, still suffer from a lack of regular data-takes and from spatially long wavelength errors related to inaccurate orbital information and long-wavelength variations in the atmosphere. It therefore remains somewhat unclear how well InSAR data can in fact resolve fault slip of large subduction earthquakes.

[4] The 11 March 2011 Tohoku-Oki megathrust earthquake in Japan provides an excellent opportunity to study the fault-slip resolution obtained by different measurement methods, as the Japanese islands are extensively instrumented with both seismic and GPS instruments. This magnitude M_w 9.0 earthquake occurred off the Pacific coast of Tohoku district in eastern Japan. It is the largest earthquake in the recent history of Japan and the fourth largest earthquake to occur in the world since 1900. This event resulted from low-angle thrust faulting on the subduction zone plate boundary (Japan Trench), which accommodates ~8–9 cm/year convergence between the Pacific and North American plates [*DeMets et al.*, 2010]. Utilizing different geophysical datasets, e.g., teleseismic, strong motion, geodetic observations and tsunami datasets, several coseismic slip distribution models have already been published [*Simons et al.*, 2011; *Ozawa et al.*, 2011; *Pollitz et al.*, 2011b; *Koketsu et al.*, 2011].

[5] The coseismic deformation of the Tohoku-Oki earthquake was recorded by hundreds of GPS stations of the nationwide GEONET and the Tohoku University GPS networks. Several researchers have already used these GPS observations to estimate both the coseismic and the postseismic slip distributions of the earthquake [*Ozawa et al.*, 2011; *Pollitz et al.*, 2011b]. InSAR has also been used to capture the coseismic deformation based on 6 parallel tracks of ascending ALOS data and on Envisat acquisitions from 3 parallel descending tracks [*Feng et al.*, 2012]. However, none of the previous studies have used InSAR observations from both ascending and descending orbits to infer the fault slip distribution of this event. Given this new data source, some important questions need to be addressed: (1) How large is the difference between fault-slip models derived from InSAR data on one hand and GPS data on the other

[1]King Abdullah University of Science and Technology (KAUST), Thuwal, Saudi Arabia.

Corresponding author: G. Feng, King Abdullah University of Science and Technology, Thuwal 23955-6900, Saudi Arabia. (fredgps@gmail.com)

0094-8276/12/2012GL051628

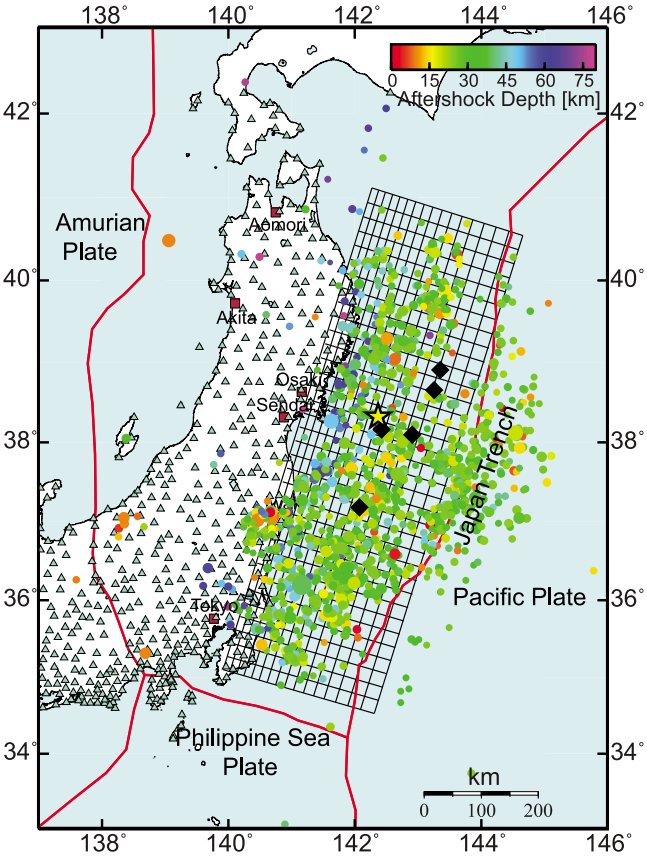

Figure 1. The model fault plane (grid) and aftershocks of the Tohoku-Oki earthquake (yellow star marks the epicenter), with circle color and size indicating the aftershock depth and magnitude. Light-blue triangles show onland GPS stations and black diamonds the seafloor GPS/acoustic stations used in this study. Red plate boundary lines are from *DeMets et al.* [2010].

hand? (2) How well we can resolve the fault slip when using InSAR data alone, without any orbital corrections from GPS? (3) What is the value of using InSAR data for studying this earthquake?

[6] In this study we first estimated 6 fault-slip distribution models for the Tohoku-Oki earthquake by using the GPS data alone, the InSAR data alone, and different combinations of the InSAR and GPS data, with or without seafloor GPS/acoustic data. We then compare the fault slip models and describe the most important differences between them. Finally, we discuss the limitations and contributions of InSAR for studying the Tohoku-Oki earthquake and for studying subduction zone earthquakes in general.

2. InSAR and GPS Datasets

[7] We used three kinds of datasets in this study: InSAR observations, onland continuous GPS data (GEONET) and seafloor GPS/acoustic data. The onland GPS displacements (Version 0.3) were provided by the ARIA research team at JPL and Caltech and are based on original GEONET RINEX GPS data from the Geospatial Information Authority (GSI) of Japan (ARIA, ARIA GPS displacement data provided by JPL and Caltech, 1 June 2011, available at ftp://sideshow.jpl.nasa.gov/pub/usrs/ARIA/). The GPS coseismic displacements were derived from the difference between position solutions at six minutes preceding and nine minutes after the mainshock. We included 551 GPS stations in our analysis, stations that cover eastern Japan and are within 600 km from the epicenter of the earthquake (Figure 1). We assumed that the vertical displacement uncertainty is two times larger than that of the horizontal components, because only the total uncertainty (sigma) was reported by the ARIA team. The seafloor displacements were derived using a GPS-acoustic technique at 5 sites, showing up to 24 m horizontal and 3 m vertical displacements [*Sato et al.*, 2011]. The uncertainty of the seafloor displacement components has been estimated to be about 0.25 m.

[8] The InSAR data consist of ALOS PALSAR data, acquired from 6 parallel ascending-orbit tracks (from T400 to T405), and of Envisat ASAR data from 3 parallel descending tracks (T347, T74 and T189). Each track is 200–700 km long and together the InSAR data capture almost the entire onland-portion of the coseismic deformation field. The post-earthquake acquisitions of these data were made 4–38 days after the mainshock. We processed the SAR data by applying the standard 2-pass differential InSAR method using the GAMMA SAR processing software package [*Wegmüller and Werner*, 1997].

[9] The InSAR data are plagued with orbital errors, causing spatially-long wavelength signals or ramps in the data. In our earlier study [*Feng et al.*, 2012], we used a 2-D quadratic model to remove the orbital errors in the interferograms based on GPS measurements, to reduce the errors in the InSAR data. Here, we used these GPS-calibrated InSAR data, but we also tested a fully independent InSAR data set that does not contain any GPS corrections. The reason is that we want to analyse how well we can resolve the fault slip with the InSAR data alone, as in many other subduction zones we may have to rely only on InSAR data.

3. Fault-Slip Modeling

[10] In the fault modeling we fixed the geometry of the fault to be consistent with the Global CMT solution, the aftershock distribution [*U.S. Geological Survey*, 2011], as well as the general orientation of the trench (Figure 1). The fault plane has a strike of 197 degrees and is about 700 km long and 320 km wide curved surface. We chose a linearly increasing fault dip from 10 degrees at the trench in the east to 20 degrees in the west, as the subduction interface progressively becomes steeper towards the west [*Miura et al.*, 2005]. We also tested a model with three fault segments that follow the Japan Trench somewhat closer, but that more complicated model did not improve the RMS misfit, so we stuck to the single curve-planar fault model. To determine finer details of the slip distribution we discretized the curved fault-plane into 20 km × 20 km fault patches and solved for both variable dip- and strike-slip for each patch, as some strike-slip is required to fit the near-fault seafloor GPS/acoustic data. We constructed the Green's functions of surface displacements assuming a homogeneous elastic half-space and a Poisson's ratio of 0.25.

[11] We reduced the 6 track ALOS data to 1432 points and the 3 track Envisat data to 821 points based on a method that considers both fringe rate and coherence. This data reduction method not only maximizes the deformation information but

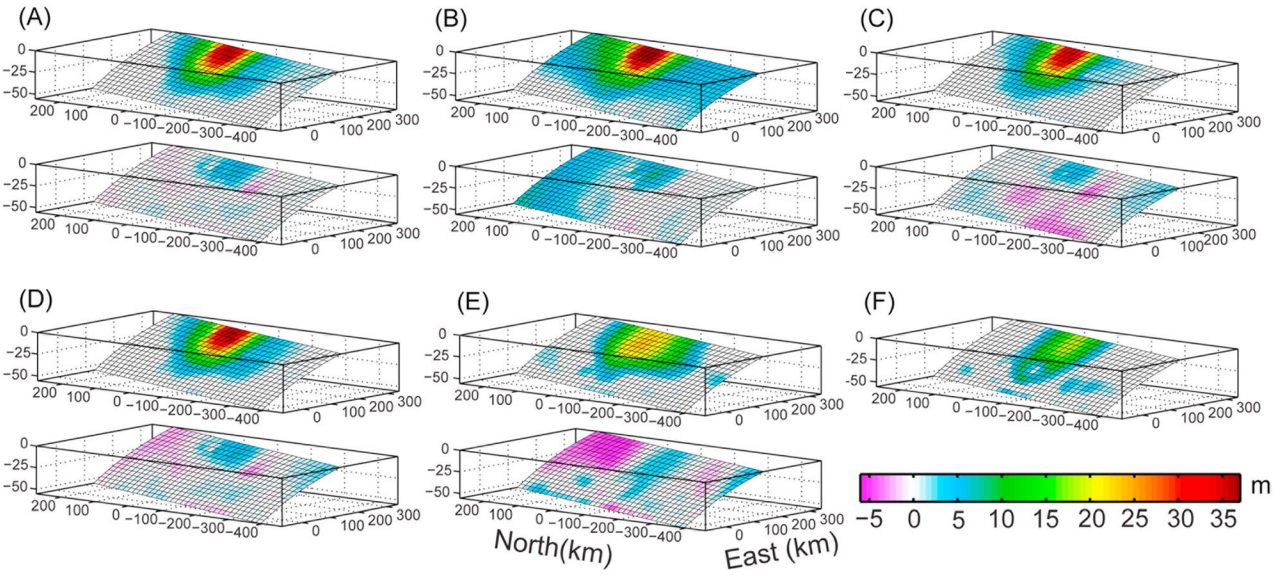

Figure 2. Variable fault slip estimated from (a) all GPS data, (b) InSAR data and seafloor GPS/acoustic data, (c) GPS-calibrated InSAR data and seafloor GPS/acoustic data, (d) all GPS and InSAR data, (e) onland GPS data and InSAR, and (f) InSAR data alone. For each model the reverse slip is shown above and strike-slip below. Positive strike-slip values represent left-lateral slip.

also ensures robustness by considering the interferometric coherence. To minimize the influence of shallow aftershocks and phase unwrapping errors, we manually removed affected data points, based on a residual map presented in our previous work [*Feng et al.*, 2012]. The relative weight factors between the two or more different types of observations, i.e., the InSAR, onland GPS and seafloor GPS/acoustic data, were chosen using a covariance component estimation of Helmert type [*Sahin et al.*, 1992]. This method is often used to combine different kinds of data with heterogeneous measurement quantities (e.g., distances and angles) or homogeneous quantities (e.g., displacements derived from different instruments, such as InSAR and GPS) in geodetic data processing.

[12] To avoid oscillatory fault-slip solutions in the modeling, we smoothed the solution using a Laplacian constraint for fault slip and used an L-curve method to choose a suitable smoothing factor [*Hansen*, 1992]. The smoothing factors were chosen to balance the roughness of fault slip and the data misfit, and adjusted for each model case such that the different models have similar fault-slip roughness. Beside the earthquake fault-slip model parameters, we included 3 additional offset parameters for the seafloor GPS/acoustic data, because these data were not calibrated to the onland GPS observations. And finally, in the case of the InSAR data without GPS calibration (models B and F in Section 4), we included 3 parameters to estimate a planar surface for each interferogram track to account for long-wavelength orbital and atmospheric delay errors.

4. Slip Distribution Model Comparisons

[13] We estimated variations in fault slip using the fault geometry and modeling approach described above, and generated 6 solutions based on 6 different sub-sets of the data: (A) all GPS data, (B) InSAR data and seafloor GPS/acoustic data, (C) GPS-calibrated InSAR data and seafloor GPS/acoustic data, (D) all GPS and InSAR data, (E) onland GPS and InSAR data, and (F) InSAR data alone. The seafloor GPS/acoustic data were included in all estimations except for models E and F. The resulting slip distributions are shown in Figure 2 and Table 1 lists the corresponding moment magnitude and average RMS values for each modeling solution.

[14] The resulting reverse-slip distributions of models A-D are very similar (Figure 2), with model B showing slightly larger maximum slip and some reverse faulting extending further north and further south, than in other models. The correlation coefficients of models A, B and C to model D for reverse slip are 0.998, 0.975, and 0.993, respectively, but lower for strike-slip, or 0.92, 0.25, and 0.62. Excluding the seafloor GPS/acoustic data (models E and F) has a dramatic

Table 1. The Moment, Magnitude and Average RMS Values for the Estimated Fault-Slip Models A–F (Figure 2)[a]

	M_o ($\times 10^{22}$ Nm)	M_w	GPS_x (cm)	GPS_y (cm)	GPS_z (cm)	Seafloor GPS/Acoustic (cm)	ALOS (cm)	Envisat (cm)
A	3.61	9.01	1.8	1.6	2.9	23	*6.5*	*8.2*
B	5.35	9.12	*33.2*	*34.7*	*9.9*	26	5.6	9.1
C	3.70	9.02	*5.1*	*19.5*	*4.0*	20	4.5	7.6
D	3.73	9.02	2.8	1.8	3.0	19	5.1	7.7
E	3.87	9.02	2.3	2.6	2.6	*198.9*	5.3	7.6
F	1.87	8.82	*44.6*	*16.3*	*4.7*	*324.7*	4.9	8.7

[a]RMS values in *italic* mark data that were not part of the corresponding fault-slip inversion.

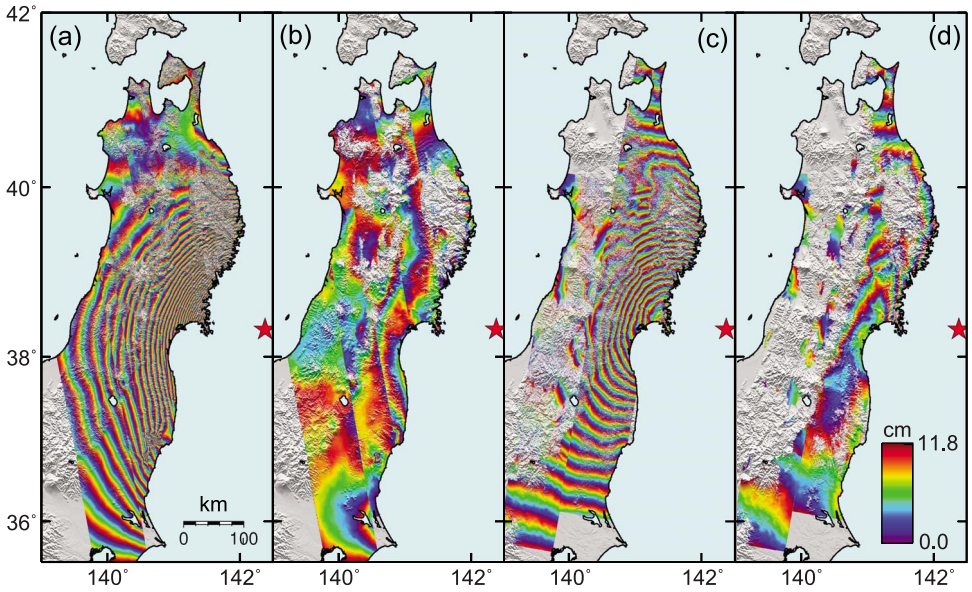

Figure 3. InSAR observations and model-prediction residuals. (a) The ascending-orbit ALOS data and (b) the residual between these observations and the GPS model A prediction. (c) The descending-orbit Envisat data and (d) the residual between the Envisat observations and the GPS model prediction. All interferograms are displayed using 11.8 cm per color-fringe.

effect, resulting in much lower maximum slip and significantly deeper location of the peak-slip (Figures 2e and 2f). This shows that the seafloor GPS/acoustic data are crucial in constraining the fault slip of this earthquake.

[15] The InSAR data appear to have significantly lower strike-slip resolution than the GPS data, even though during the data reduction process we avoided including unreliable InSAR data located near shallow aftershocks, phase unwrapping errors, and un-modeled orbital errors. The main reason for the poor strike-slip resolution is that strike-slip in this case is mainly constrained by observed north-south displacements, to which the InSAR line of sight (LOS) observation is not so sensitive. The central-track LOS unit vector components [east, north, up] for the ascending ALOS and descending Envisat observations are [−0.61, −0.11, 0.78] and [0.65, −0.11, 0.75], confirming the limited north-south sensitivity. In fact, the sensitivity is so low, that when using InSAR data alone in the modeling (model F) we had to constrain the strike-slip to zero, as otherwise the resulting model would have unrealistically large strike-slip.

[16] In order to make quantitative comparisons between the different models, we calculated RMS values of each model prediction for all the data sets (Table 1). By this we can test how well, e.g., the InSAR derived model does in fitting the GPS data and thus identify important differences between the models. The InSAR model prediction (model B), for example, results in poor GPS RMS values of 33.2 cm, 34.7 cm and 9.9 cm for the east, north and up components, respectively (Table 1). These RMS values improve to 5.1 cm, 19.5 cm, and 4.0 cm when the GPS-calibrated InSAR data are used (model C), showing that this model fits the east and up components well, but not the north component, due to the poor InSAR sensitivity to north-south displacements, described above. The large improvement of model C in fitting the GPS data highlights the seriousness of the long-wavelength errors in the InSAR data. In contrast to models B and C, the GPS-only model prediction (model A) fits the GPS-corrected InSAR observations very well, as indicated by the small InSAR residual (Figure 3 and Table 1) leaving only some postseismic and shallow aftershock deformation, plus some phase unwrapping, un-modeled orbital, and atmospheric errors.

5. Discussion and Conclusions

[17] The comparison between the different fault-slip distribution models above, shows that the GPS-only model A is very similar to the joint model D, for both dip slip and strike slip (Figure 2). Furthermore, the predicted ground displacements calculated from the GPS model A fit both the ascending ALOS and descending Envisat InSAR observations very well. This means that there is no real gain by including the InSAR observations for determining the fault slip distribution of this earthquake. Another point of evidence for this conclusion is the fact that the InSAR observations can even be directly simulated from interpolating the GPS observations [*Feng et al.*, 2012]. Finally, the InSAR observations include postseismic deformation and shallow aftershock deformation, as well as more significant errors than the GPS data, related to inaccurate orbital information and unwrapping problems. These errors and the post-earthquake deformation lead to a biased estimate of the coseismic fault slip distribution when InSAR data are used alone.

[18] Even though the extensive InSAR observations do not help in determining the coseismic slip distribution of this earthquake, we can benefit from using the InSAR data in at least two important ways. First, we used the InSAR data to identify anomalous GPS stations in the coseismic deformation field [*Feng et al.*, 2012]. It is generally difficult to identify anomalous GPS observations from other GPS data, especially when the density of GPS stations is not very high or if distribution of stations is not uniform. The high spatial-resolution nature of the InSAR observations therefore helped to validate the GPS observations, eliminate erroneous GPS

displacements, and made the GPS data cleaner and more robust for the modeling. Second, the InSAR observations provide details of the deformation caused by shallow on-land aftershocks, which caused significant displacements at only a few stations within the GPS network. Therefore, the InSAR observations can be used to study the fault geometry, slip, and other aspects of those aftershocks [*Fukushima et al.*, 2011].

[19] InSAR has proven to be extremely useful for many earthquake studies, especially for shallow and surface-rupturing on-land earthquakes, as InSAR can provide high spatial resolution phase and offset tracking observations of the coseismic deformation [*Simons and Rosen*, 2007]. However, when studying subduction zone earthquakes, InSAR suffers from its shortcomings, and can even be of limited or no use when a dense GPS network exists, because subduction earthquake deformation is generally of large-scale and so smooth that good GPS networks easily capture it. In addition, many subduction earthquakes occur far off-shore, resulting in limited on-land deformation. Nevertheless, InSAR observations are commonly used as the primary data to constrain slip distribution models, due to limited GPS station coverage, e.g., in the 2010 M_w 8.8 Maule, Chile earthquake [*Pollitz et al.*, 2011a].

[20] In most subduction zones, land-based geodetic data are limited and InSAR observations are often the main or even the only available data for studying coseismic deformation of subduction zone earthquakes [*Pollitz et al.*, 2011a]. Therefore, the spatially long-wavelength errors in InSAR data, e.g., due to inaccurate orbital information and long-wavelength atmospheric delays, cannot usually be corrected for using GPS data. Model F shows that we can derive some of the main fault slip characteristics using the InSAR data alone, if we estimate ramp corrections along with the fault-slip parameters. Using quadratic or higher order ramp corrections will result in large trade-offs between ramp parameters and fault slip, so planar corrections should be used. This Tohoku-Oki example also shows that despite using both ascending and descending InSAR observations, the sensitivity to strike-slip is so low, that we had to constrain it to zero to avoid large unrealistic strike-slip values. While the sensitivity to strike slip depends on the orientation of the plate boundary, our results indicate that when using InSAR data alone in constraining fault slip of subduction zone earthquakes, one should use information from seismology in the modeling, such as mean-rake and minimum-moment constraints.

[21] To understand better the cause for the poor performance of the InSAR data we estimated two additional fault-slip models. We selected the GPS stations that fall within the area covered by the InSAR tracks and converted the three-dimensional GPS data into ascending and descending LOS displacements. We then estimated the fault slip using these LOS data as they were normal InSAR data (model B2) and also as ramp-free InSAR data (model C2). The GPS RMS values in (x, y, z) for these new models B2 and C2 are (7.8 cm, 16.8 cm, 8.0 cm) and (4.1 cm, 15.2 cm, 5.3 cm), respectively. The similarity between the GPS residuals of models C and C2 shows that the InSAR data were successfully GPS-calibrated in case C, but the residuals are still large, highlighting the limitations of the InSAR imaging geometry. The RMS values in case B2 are significantly larger than for C2, which indicates that there is a trade-off between ramp parameters and fault slip. And finally, the very large GPS residuals of model B demonstrate how serious long-wavelength errors in InSAR data can be, as discussed above. The orbital information for new and upcoming radar satellites is and will be better than for ALOS and Envisat [e.g., *Yoon et al.*, 2009]. In addition, long-wavelength atmospheric signals are also increasingly being corrected for in InSAR data using weather models [e.g., *Jolivet et al.*, 2011]. Therefore, long-wavelength errors in InSAR data should become less of a problem in the future. The limitations of InSAR imaging geometry, however, remain as long as radar satellites are only operated in polar orbits, although they may be partially over-come by using azimuth pixel offsets or split-beam (multiple-aperture) interferometry [*Bechor and Zebker*, 2006].

[22] Because of the limited gain of including InSAR observations for determining the fault slip distribution of the Tohoku-Oki earthquake and as the GPS data include less postseismic and aftershock deformation, we choose the GPS model A as our final fault-slip model. This model suggests that maximum reverse faulting of ~36 m took place above 10 km depth on the megathrust offshore, and that most of the slip is confined to the uppermost part of the plate boundary, above 30 km depth. Our result broadly agrees with previously published geodetic inversion results [*Ozawa et al.*, 2011; *Pollitz et al.*, 2011b], teleseismic results [*Tsai et al.*, 2011] and with fault-slip solutions based on joint inversions of GPS, seismic, and tsunami data [*Simons et al.*, 2011; *Koketsu et al.*, 2011]. The estimated coseismic high-slip region laterally coincides with the location of high seismic coupling derived from interseismic crustal velocity measurements from before the earthquake [*Hashimoto et al.*, 2009; *Loveless and Meade*, 2011]. However, the high-slip is located well up-dip of that highly coupled area, which probably is a reflection of the limited resolution of the interseismic coupling estimation on the uppermost part of the plate interface, rather than indicating that this part of the fault was poorly coupled before the earthquake.

[23] In summary, we have estimated the fault slip distribution of the great 11 March, 2011 Tohoku-Oki earthquake using six combinations of different datasets. We compared the resulting models to find that the InSAR observations do not add anything for determining the coseismic fault slip distribution this earthquake. Our final preferred solution includes both reverse faulting and strike slip. The maximum reverse- and strike-slip values are 36.0 m and 6.0 m, respectively, located at a shallow depth of 6 km, northeast of the epicenter. The total geodetic moment is 3.6×10^{22} Nm (M_w 9.01), similar to seismological estimates.

[24] **Acknowledgments.** The GPS displacements (Version 0.3) were provided by the ARIA team at JPL based on GPS data from the Geospatial Information Authority (GSI) of Japan. The ALOS PALSAR data were provided by the Japan Aerospace Exploration Agency (JAXA), Project P517, and the GEO Geohazards Supersite. The Envisat ASAR data were supplied through the GEO Geohazards Supersite. We thank Xiaoli Ding and Zhiwei Li for helping out with the InSAR data and the data processing. This paper was improved by constructive comments from Jeff Freymueller and one anonymous reviewer.

[25] The Editor thanks Jeffrey Freymueller and anonymous reviewer for assisting with the evaluation of this paper.

References

Bechor, N. B. D., and H. A. Zebker (2006), Measuring two-dimensional movements using a single InSAR pair, *Geophys. Res. Lett.*, *33*, L16311, doi:10.1029/2006GL026883.

DeMets, C., R. G. Gordon, and D. F. Argus (2010), Geologically current plate motions, *Geophys. J. Int.*, *181*(1), 1–80, doi:10.1111/j.1365-246X.2009.04491.x.

Feng, G., et al. (2012), Calibration of an InSAR-derived coseismic deformation map associated with the 2011 Mw-9.0 Tohoku-Oki earthquake, *IEEE Geosci. Remote Sens. Lett.*, *9*(2), 302–306, doi:10.1109/LGRS.2011.2168191.

Fukushima, Y., Y. Takada, T. Ozawa, and M. Hashimoto (2011), ALOS/PALSAR observations associated with the 2011 Mw 9.0 Tohoku, Japan, earthquake, Abstract G44A-05 presented at 2011 Fall Meeting, AGU, San Francisco, Calif., 5–9 Dec.

Hansen, P. C. (1992), Analysis of discrete ill-posed problems by means of the L-curve, *SIAM Rev.*, *34*, 561–580, doi:10.1137/1034115.

Hashimoto, C., A. Noda, T. Sagiya, and M. Matsuura (2009), Interplate seismogenic zones along the Kuril-Japan trench inferred from GPS data inversion, *Nat. Geosci.*, *2*, 141–144, doi:10.1038/ngeo421.

Jolivet, R., R. Grandin, C. Lasserre, M.-P. Doin, and G. Peltzer (2011), Systematic InSAR tropospheric delay corrections from global meteorological reanalysis data, *Geophys. Res. Lett.*, *38*, L17311, doi:10.1029/2011GL048757.

Koketsu, K., et al. (2011), A unified source model for the 2011 Tohoku earthquake, *Earth Planet. Sci. Lett.*, *310*(3–4), 480–487, doi:10.1016/j.epsl.2011.09.009.

Lorito, S., et al. (2011), Limited overlap between the seismic gap and coseismic slip of the great 2010 Chile earthquake, *Nat. Geosci.*, *4*, 173–177, doi:10.1038/ngeo1073.

Loveless, J. P., and B. J. Meade (2011), Spatial correlation of interseismic coupling and coseismic rupture extent of the 2011 M_W = 9.0 Tohoku-oki earthquake, *Geophys. Res. Lett.*, *38*, L17306, doi:10.1029/2011GL048561.

Miura, S., et al. (2005), Structural characteristics off Miyagi forearc region, the Japan Trench seismogenic zone, deduced from a wide-angle reflection and refraction study, *Tectonophysics*, *407*, 165–188, doi:10.1016/j.tecto.2005.08.001.

Ozawa, S., et al. (2011), Coseismic and postseismic slip of the 2011 magnitude-9 Tohoku-Oki earthquake, *Nature*, *475*, 373–376, doi:10.1038/nature10227.

Pollitz, F. F., et al. (2011a), Coseismic slip distribution of the February 27, 2010 Mw 8.8 Maule, Chile earthquake, *Geophys. Res. Lett.*, *38*, L09309, doi:10.1029/2011GL047065.

Pollitz, F. F., R. Bürgmann, and P. Banerjee (2011b), Geodetic slip model of the 2011 M9.0 Tohoku earthquake, *Geophys. Res. Lett.*, *38*, L00G08, doi:10.1029/2011GL048632.

Sahin, M., P. A. Cross, and P. C. Sellers (1992), Variance component estimation applied to satellite laser ranging, *Bull. Geod.*, *66*, 284–295, doi:10.1007/BF02033189.

Sato, M., et al. (2011), Displacement above the hypocenter of the 2011 Tohoku-Oki earthquake, *Science*, *332*(6036), 1395, doi:10.1126/science.1207401.

Simons, M., and P. Rosen (2007), Interferometric synthetic aperture radar geodesy, in *Treatise on Geophysics*, vol. 3, *Geodesy*, edited by G. Schubert, pp. 391–446, Elsevier, Amsterdam, doi:10.1016/B978-044452748-6.00059-6.

Simons, M., et al. (2011), The 2011 magnitude 9.0 Tohoku-Oki earthquake: Mosaicking the megathrust from seconds to centuries, *Science*, *332*(6036), 1421–1425, doi:10.1126/science.1206731.

Tong, X., et al. (2010), The 2010 Maule, Chile earthquake: Downdip rupture limit revealed by space geodesy, *Geophys. Res. Lett.*, *37*, L24311, doi:10.1029/2010GL045805.

Tsai, V. C., G. P. Hayes, and Z. Duputel (2011), Constraints on the long-period moment-dip tradeoff for the Tohoku earthquake, *Geophys. Res. Lett.*, *38*, L00G17, doi:10.1029/2011GL049129.

U.S. Geological Survey (2011), Magnitude 9.0 near the east coast of Honshu Japan, report, Denver, Colo. [Available at http://earthquake.usgs.gov/earthquakes/eqinthenews/2011/usc0001xgp/.]

Wegmüller, U., and C. L. Werner (1997), Gamma SAR processor and interferometry software, in *Proceedings of the 3rd ERS Symposium, Eur. Space Agency Spec. Publ., ESA SP-414*, 1686–1692.

Yoon, Y. T., et al. (2009), TerraSAR-X precise trajectory estimation and quality assessment, *IEEE Trans. Geosci. Remote Sens.*, *47*(6), 1859–1868, doi:10.1109/TGRS.2008.2006983.